RSC Advances

PAPER

View Article Online
View Journal | View Issue

Cite this: *RSC Adv.*, 2022, **12**, 21742

L-Asparagine–EDTA–amide silica-coated MNPs: a highly efficient and nano-ordered multifunctional core–shell organocatalyst for green synthesis of 3,4-dihydropyrimidin-2(1*H*)-one compounds†

Negin Rostami, Mohammad G. Dekamin,* Ehsan Valiey and Hamidreza FaniMoghadam

In this study, new L-asparagine grafted on 3-aminopropyl-modified Fe_3O_4@SiO_2 core–shell magnetic nanoparticles using the EDTA linker (Fe_3O_4@SiO_2–APTS–EDTA–asparagine) was prepared and its structures properly confirmed using different spectroscopic, microscopic and magnetic methods or techniques including FT-IR, EDX, XRD, FESEM, TEM, TGA and VSM. The Fe_3O_4@SiO_2–APTS–EDTA–asparagine core–shell nanomaterial was found, as a highly efficient multifunctional and recoverable organocatalyst, to promote the efficient synthesis of a wide range of biologically-active 3,4-dihydropyrimidin-2(1*H*)-one derivatives under solvent-free conditions. It was proved that Fe_3O_4@SiO_2–APTS–EDTA–asparagine MNPs, as a catalyst having excellent thermal and magnetic stability, specific morphology and acidic sites with appropriate geometry, can activate the Biginelli reaction components. Moreover, the environmental-friendliness and nontoxic nature of the catalyst, cost effectiveness, low catalyst loading, easy separation of the catalyst from the reaction mixture and short reaction time are some of the remarkable advantages of this green protocol.

Received 9th May 2022
Accepted 3rd July 2022

DOI: 10.1039/d2ra02935a

rsc.li/rsc-advances

Introduction

Green and sustainable chemistry has played a key role in both academia and chemical industry for a better life and future.[1–8] In this regard, heterogeneous catalytic systems and their magnetic nanoparticle (MNP) counterparts have received considerable interest because of their unique properties.[9–11] The outstanding properties of MNPs have made them superior and indispensable in many areas of academia and industry including information storage,[12] medicine,[13] drug delivery,[14] magnetic resonance imaging (MRI),[15–17] biomedical applications,[10,18,19] and environmental remediation[20] as well as heterogeneous catalysis.[21–24] In academia, MNPs represent a promising new tool for performing chemical reactions because they are separated from the reaction medium, comfortably.[25,26] In industry, due to importance of the cost of chemical processes and reusing of the catalysts, special attention is paid to these nanoparticles.[27,28] However, MNPs tend to agglomerate under a magnetic field that reduces their surface to volume ratio and consequently decreases catalytic activity.[29] Therefore, MNPs must be stabilized to improve their properties and prevent undesirable agglomeration.[30,31] In fact, they are coated with a protective layer such as carbon layers,[32,33] organic polymers[34] or silica.[35–37]

Moreover, multi-component reactions (MCRs) are the most desirable powerful synthetic route in which three or more reactants come together in a single reaction vessel to form a wide range of acyclic or heterocyclic compounds by one-pot processes.[38–41] MCRs afford extended molecular complexity and diversity from simple starting materials with high atom economy, which have found applications in medicinal and natural products chemistry.[42,43] Indeed, the most significant feature of MCRs is generating almost no by-products or simple molecules such as H_2O or EtOH.[44–48] Hence, in agreement of the green and sustainable chemistry process, development and the advancement of catalysts to promote MCRs are very important in synthetic and medicinal chemistry.[49–51]

Among the various types of nitrogen-containing heterocycles, derivatives of 3,4-dihydropyrimidin-2(1*H*)-one, as biologically-active compounds, have found versatile applications such as anti-bacterial, anti-inflammatory, antihypertensive agents, calcium channel blockers and antitumor compounds.[52–60] A simple and general protocol for access to 3,4-dihydropyrimidin-2(1*H*)-ones involves the three-component and one-pot Biginelli cyclocondensation of ethyl acetoacetate, urea and various aldehydes accelerated by different types of acidic catalytic systems such as copper(II)

Pharmaceutical and Biologically-Active Compounds Research Laboratory, Department of Chemistry, Iran University of Science and Technology, Tehran 16846-13114, Iran. E-mail: mdekamin@iust.ac.ir; Fax: +98-21-7730 21584; Tel: +98-21-77 240 284

† Electronic supplementary information (ESI) available. See https://doi.org/10.1039/d2ra02935a

trifluoromethanesulfonate under microwave irradiation,[61] gallium(III) triflate,[62] bismuth pyromanganate nanoparticles,[63] L-proline methyl ester hydrochloride,[64] nanometasilica disulfuric acid,[65] *p*-toluenesulfonic acid,[66,67] sulfonic acid-supported polymeric catalysts,[68] sulfonated carbons from agro-industrial wastes,[69] phenylboronic acid,[70] 1,3-bis(carboxymethyl) imidazolium chloride,[71] sulfonic acid and ionic liquid functionalized covalent organic frameworks,[72] ionic liquid combined with acidic zeolite-supported heteropolyacids,[73] ionic liquid/silica sulfuric acid,[74] bentonite/PS-SO_3H nanocomposite,[75] dendrimer-attached phosphotungstic acid immobilized on nanosilica under ultrasonication,[76] tungsten-

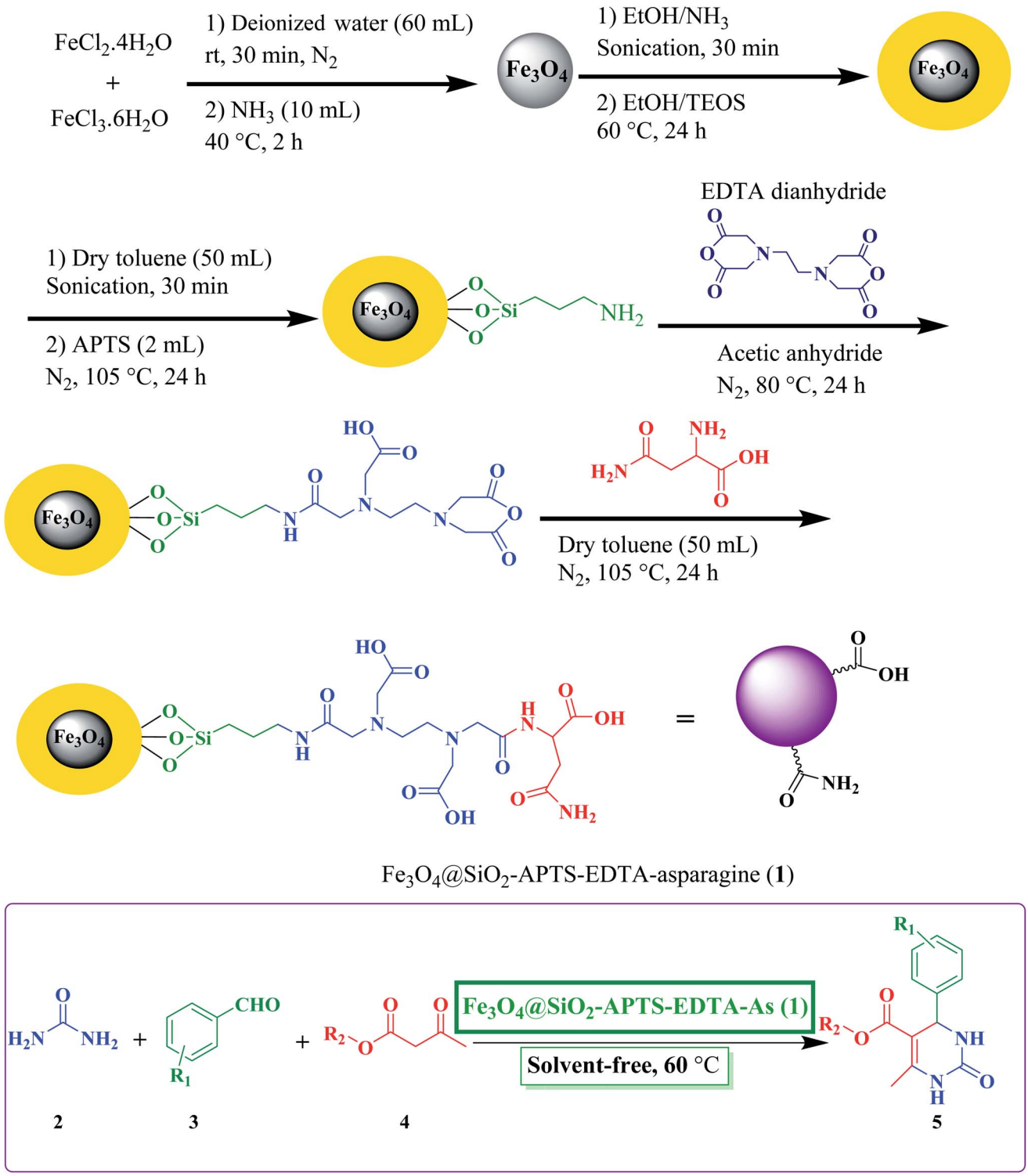

Scheme 1 Schematic preparation of Fe_3O_4@SiO_2–APTS–EDTA–asparagine (**1**), as a heterogeneous nanocatalyst, for the synthesis of 3,4-dihydropyrimidin-2(1*H*)-one **5** derivatives.

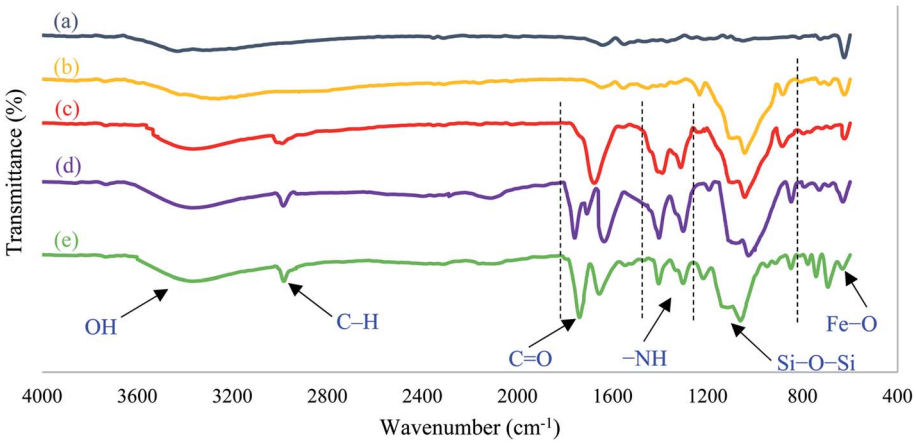

Fig. 1 FT-IR spectra of the Fe_3O_4 (a), Fe_3O_4@SiO_2 (b), Fe_3O_4@SiO_2–APTS (c), Fe_3O_4@SiO_2–APTS–EDTA (d) and Fe_3O_4@SiO_2–APTS–EDTA–asparagine (**1**, e).

substituted molybdophosphoric acid impregnated with kaolin,[53] zinc- and cadmium-based coordination polymers,[77] metal–organic frameworks (MOFs),[78,79] montmorillonite clay,[80] magnetic nanoparticles,[81] Lewis acidic zirconium(IV)–salophen perfluorooctanesulfonate or sulfated polyborate,[82,83] nanocrystalline CdS thin film,[59] graphene oxide,[84,85] and mesoporous materials.[86,87] Most of the reported methods in this regard demonstrate valuable role of heterogeneous catalysts. However, these protocols have problems such as complicated and tedious procedures or the use of corrosive as well as toxic reagents for preparation of the catalysts, long reaction times or low yields. Therefore, there is still room to develop more environmentally-benign protocols to promote the Biginelli MCR condensation using catalytic systems associated with new emerging research areas including organocatalysis.[21,88–92]

In many previous reports, ethylenediaminetetraacetic acid (EDTA) has been used as an ion exchange and chelating agent for various metal ions,[93–95] but this compound has a good ability as an inexpensive and non-toxic cross-linker to make strong bonds with organic materials having nucleophilic centers.[96,97] On the other hand, L-asparagine is one of the 20 amino acids found in the cells of the human body and is essential for maintaining balance in the central nervous system.[98] L-Asparagine can act as a biocompatible precursor and key part of bifunctional organocatalytic systems due to its high natural abundance and cost-effectiveness with acidic and basic sites.[99,100]

In continuation of our ongoing research toward development of various catalytic systems for green synthesis of different heterocyclic scaffolds,[40,101–104] we herein report the synthesis and characterizations of new L-asparagine grafted on the 3-aminopropyl-modified Fe_3O_4@SiO_2 core–shell magnetic nanoparticles using the EDTA linker (Fe_3O_4@SiO_2–APTS–EDTA–asparagine), as a magnetically recoverable organocatalyst

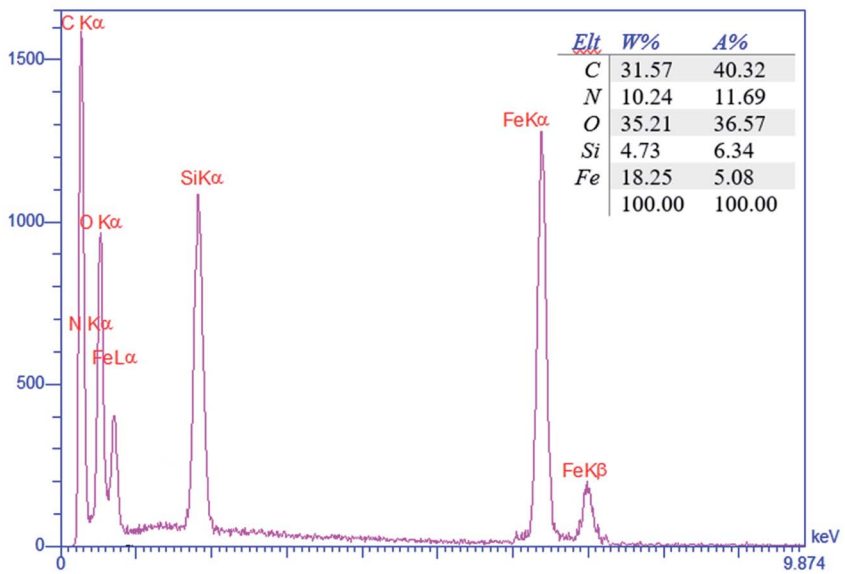

Fig. 2 The EDX spectra of the magnetic Fe_3O_4@SiO_2–APTS–EDTA–asparagine nanomaterial (**1**).

having excellent thermal and magnetic stability, and specific morphology as well as acidic and basic sites with proper geometry,[122,123] to promote the Biginelli reaction efficiently under solvent-free conditions at 60 °C (Scheme 1).

Results and discussion

Characterization of the Fe_3O_4@SiO_2–APTS–EDTA–asparagine nanocatalyst (1)

The overall procedure for the synthesis of Fe_3O_4@SiO_2–APTS–EDTA–asparagine (**1**) has been summarized in Scheme 1. At first, the obtained magnetic nanoparticles were characterized using different physicochemical techniques such as Fourier transform infrared (FT-IR) spectroscopy, energy-dispersive X-ray (EDX) spectroscopy, field emission scanning electron microscopy (FESEM), transmission electron microscopy (TEM), X-ray diffraction spectroscopy (XRD), vibrating sample magnetometer (VSM), and thermogravimetric analysis (TGA).

The FT-IR spectroscopy was employed to determine the functional groups and structure of Fe_3O_4 (a), Fe_3O_4@SiO_2 (b), Fe_3O_4@SiO_2–APTS (c), Fe_3O_4@SiO_2–APTS–EDTA (d) and Fe_3O_4@SiO_2–APTS–EDTA–asparagine (e). The results are presented in Fig. 1. In the spectra of Fe_3O_4 nanoparticles (Fig. 1a) the bands displayed at 620 cm^{-1} and about 3410 cm^{-1} are attributed to stretching vibration of Fe–O bond and surface hydroxyl groups, respectively. These peaks were observed in all five samples isolated at different synthetic steps. In the FT-IR spectrum of Fe_3O_4@SiO_2 (Fig. 1b), the absorption bands at 881 and 1036 cm^{-1} can be ascribed to the presence of Si–O–Si symmetric and Si–O–Si asymmetric stretching modes, reflecting the coating of silica layer on the magnetite nanoparticles.[105] SP^3 C–H stretching vibrations at about 2922 cm^{-1} confirmed the

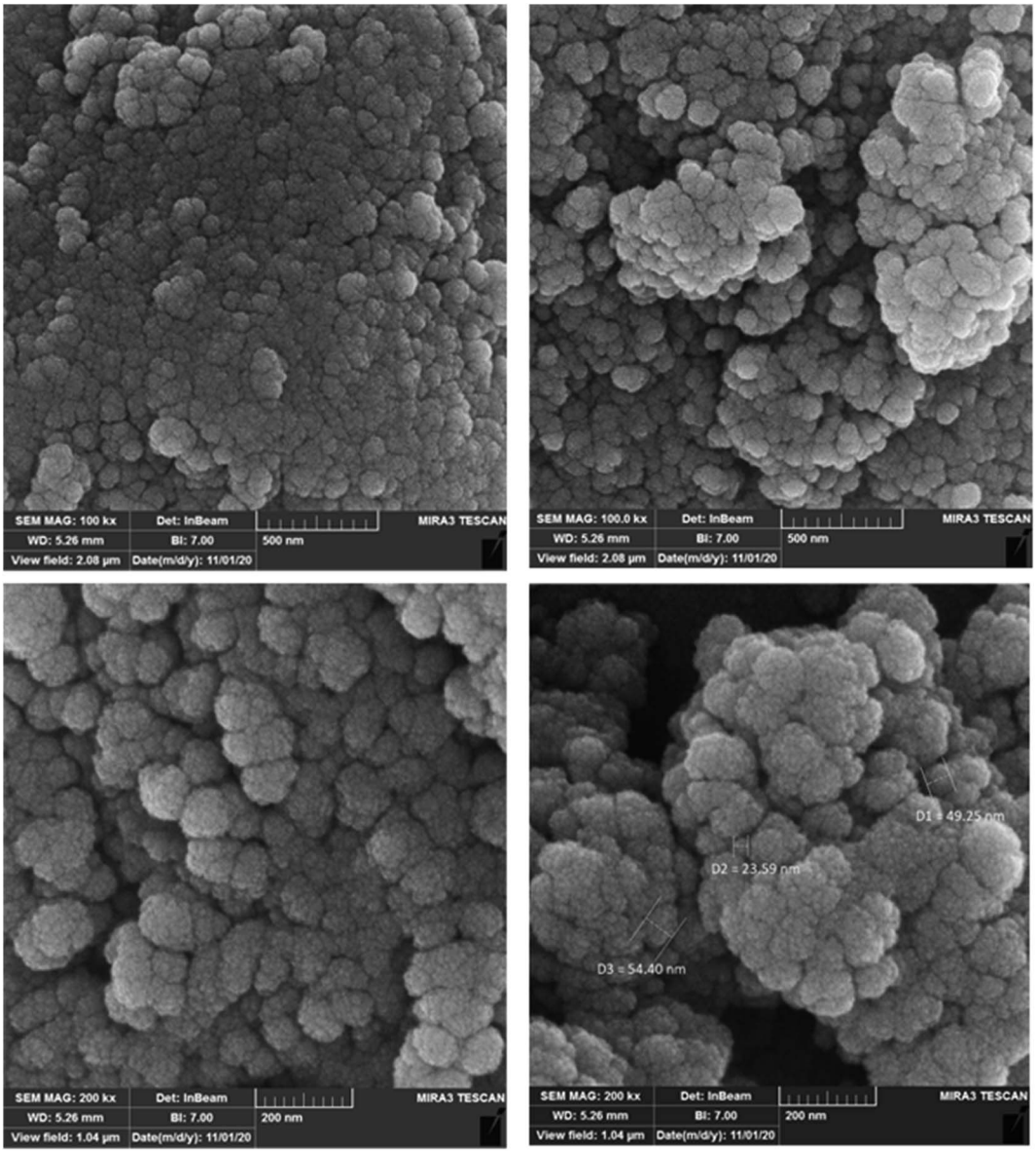

Fig. 3 FESEM images of the magnetic Fe_3O_4@SiO_2–APTS–EDTA–asparagine nanocatalyst (**1**).

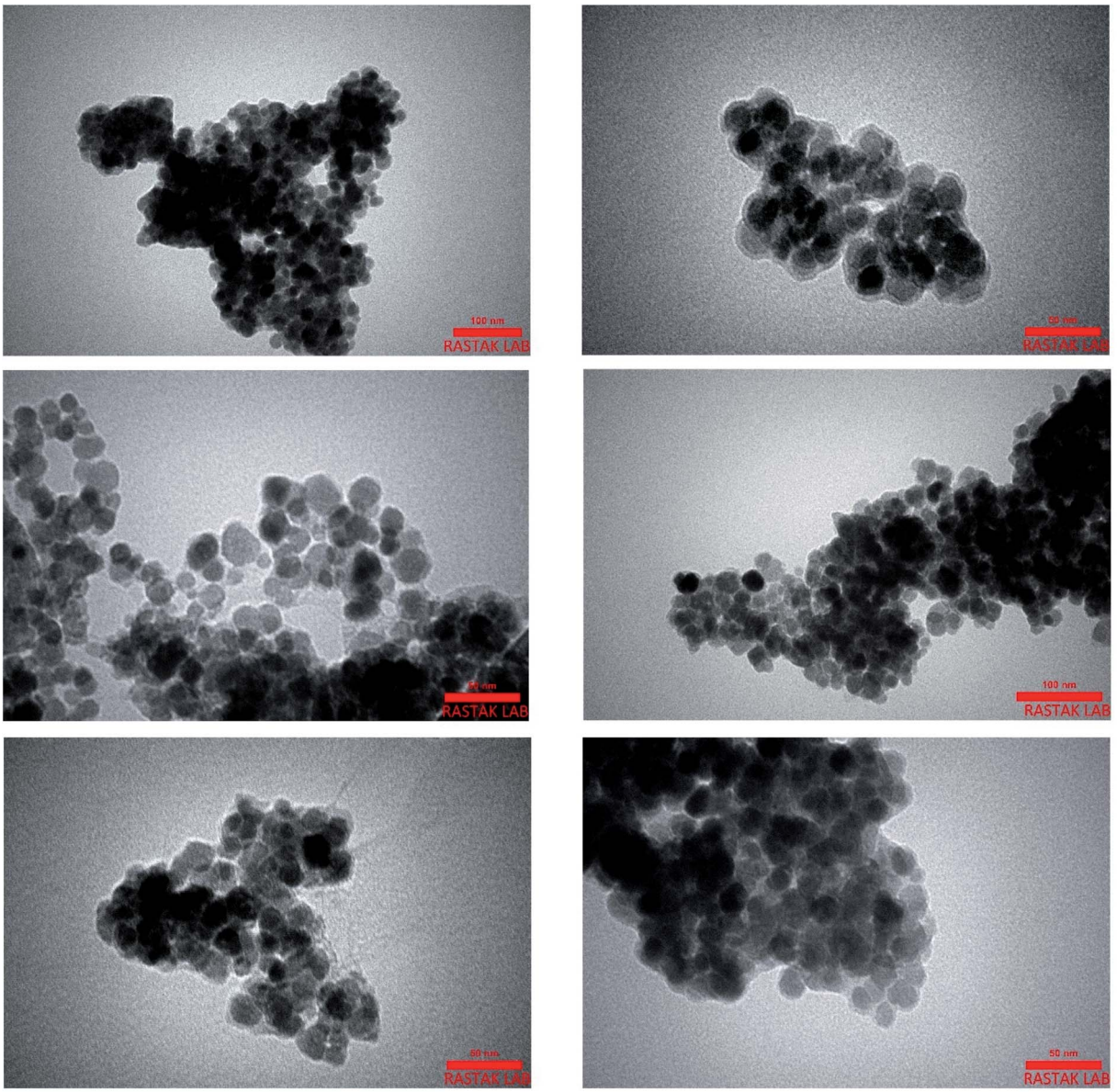

Fig. 4 TEM images of the magnetic Fe_3O_4@SiO_2–APTS–EDTA–asparagine nanomaterial (**1**).

presence of the anchored (3-aminopropyl)triethoxysilane (APTS) group and the band at about 1400 cm^{-1} is assigned to the bending of –NH groups of Fe_3O_4@SiO_2–APTS MNPs (Fig. 1c).[106] In the FT-IR spectrum of Fe_3O_4@SiO_2–APTS–EDTA (Fig. 1d), the peaks at 1635 cm^{-1}, 1707 cm^{-1} and 1760 cm^{-1} are corresponding to the C=O vibration of amide, acid and anhydride groups, respectively. In the last step, the peak at 1760 cm^{-1}, which belongs to the anhydride group has been removed and new peaks at 1651 cm^{-1} and 1737 cm^{-1} are attributed to the amide and acid groups on the surface of Fe_3O_4@SiO_2–APTS–EDTA–asparagine (Fig. 1e). These results from the FT-IR spectrum confirm that the silica coating and subsequent steps have been successfully performed on the surface of Fe_3O_4.

Compositional analysis of the Fe_3O_4@SiO_2-APTS-EDTA-asparagine magnetic nanocatalyst (**1**) was carried out using energy-dispersive X-ray spectroscopy (EDX). The EDX spectra of the Fe_3O_4@SiO_2–APTS–EDTA–asparagine nanomaterial (**1**) are depicted in Fig. 2. In addition, the EDX analysis showed the well-defined peaks related to C, O, N, Si and Fe in the structure of Fe_3O_4@SiO_2–APTS–EDTA–asparagine (**1**) with the percentages of 40.32, 36.57, 11.69, 6.34 and 5.08, respectively.

The morphology and texture of Fe_3O_4@SiO_2–APTS–EDTA–asparagine MNPs (**1**) were indicated by FESEM analysis and their photographs have been presented in Fig. 3. According to these FESEM photographs, the size and shape of nanoparticles are well observed, which proves that the particles are spherical and without agglomeration. The FESEM photographs supported the formation of spherically shaped MNPs, which is in accordance with TEM analysis.

The TEM analysis of the Fe_3O_4@SiO_2–APTS–EDTA–asparagine (**1**) MNPs in two scales is shown in Fig. 4. The TEM images demonstrated the structural order and morphology suggesting

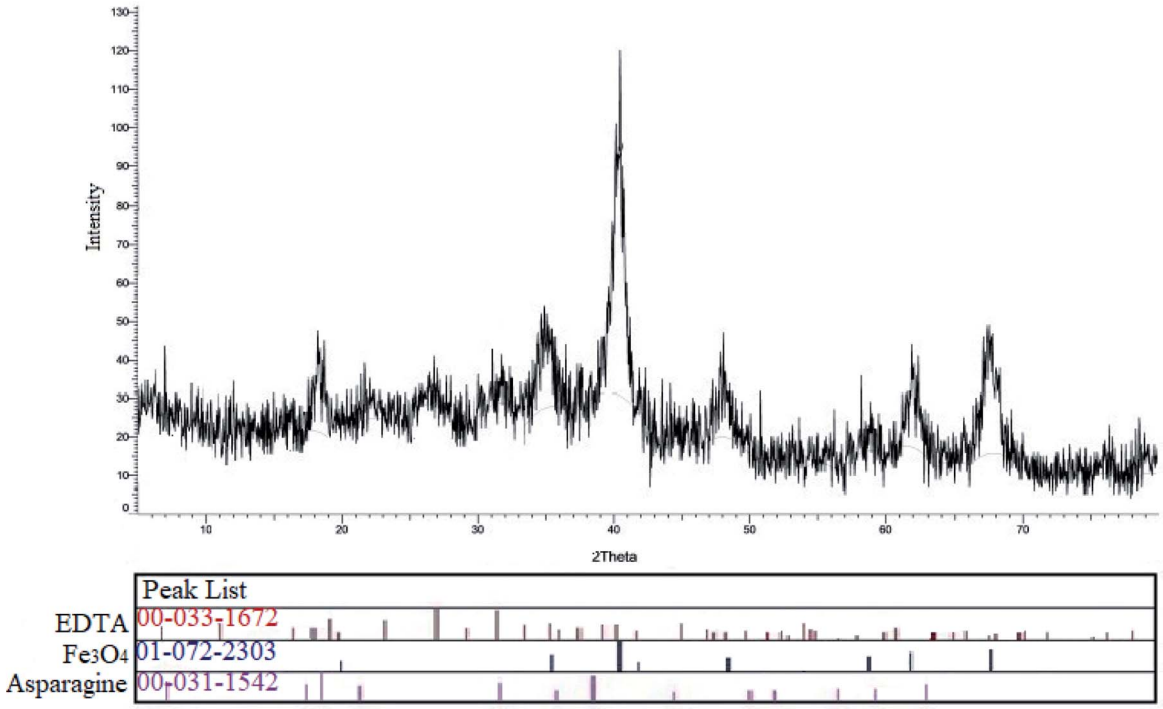

Fig. 5 XRD pattern of the magnetic Fe_3O_4@SiO_2–APTS–EDTA–asparagine nanocatalyst (**1**).

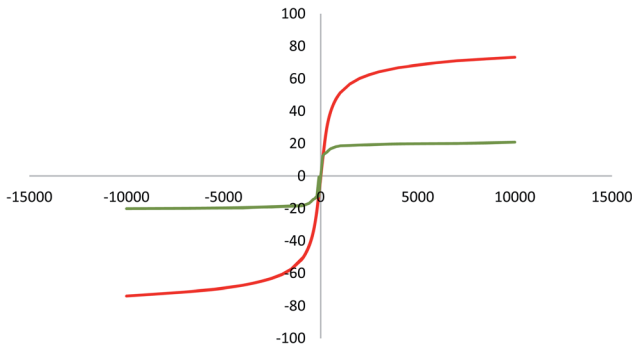

Fig. 6 VSM pattern of the Fe_3O_4 (red curve) and magnetic Fe_3O_4@SiO_2–APTS–EDTA–asparagine nanocatalyst (**1**, green curve).

that the magnetite nanoparticles have an average diameter size of 41 nm.

The XRD pattern of Fe_3O_4@SiO_2–APTS–EDTA–asparagine (**1**) was shown in Fig. 5. The reflection peaks were compared with the reference standard patterns related to EDTA (card no. JCPDS, 00-033-1672), Fe_3O_4 (card no. JCPDS, 01-072-2303) and L-asparagine (card no. JCPDS, 00-031-1542). The sharp peaks in this pattern are generated by combining several peaks. These new sharp peaks are ascribed to the produced Fe_3O_4@SiO_2–APTS–EDTA–asparagine MNPs structures after modification reactions by EDTA and L-asparagine, respectively.

The magnetic properties of MNPs were measured *via* vibrating sample magnetometry (VSM). The magnetic attributes of Fe_3O_4 and Fe_3O_4@SiO_2–APTS–EDTA–asparagine MNPs (**1**) were measured out at room temperature by applied magnetic field −1000 to +1000 oersted. According to data presented in Fig. 6, the values of magnetization saturation (Ms) for Fe_3O_4 and Fe_3O_4@SiO_2–APTS–EDTA–asparagine MNPs (**1**) are 73.12 and 20.84 emu g^{-1}, respectively. Moreover, the VSM curves of both samples exhibit no hysteresis loops and this property demonstrated that no aggregation occurred in the presence of magnetic field. A decrease in the magnetic saturation of the Fe_3O_4@SiO_2–APTS–EDTA–asparagine was observed after coating with SiO_2 and functionalization with APTS. However, the magnetic saturation of Fe_3O_4@SiO_2–APTS–EDTA–asparagine (**1**) is sufficient to be recovered by exerting an external magnet.

Thermal stability of the Fe_3O_4@SiO_2–APTS–EDTA–asparagine nanomaterial (**1**) was investigated under the air atmosphere over the temperature range of 50–800 °C (Fig. 7). The Fe_3O_4@SiO_2–APTS–EDTA–asparagine MNPs (**1**) display three weight loss steps over the temperature range of TGA and the total weight loss of nanocatalyst **1** is around 60%. According to obtained results, in the first step 15% weight loss in the range of 150–200 °C is due to the evaporation of adsorbed water and organic solvents that remain in the nanocatalyst through its preparation steps. In addition, 22% weight loss in the range of 200–400 °C corresponds to the loss of EDTA–asparagine moiety. In the last step, the sharp weight loss of 23% at 400–700 °C can be assigned to the decomposition of APTS moiety in the MNPs framework. These results also indicate that APTS, EDTA and L-asparagine have been successfully grafted onto the surface of Fe_3O_4@SiO_2. Above 700 °C only Fe_3O_4 was present.

Optimization of conditions in the Biginelli reaction using Fe_3O_4@SiO_2–APTS–EDTA–asparagine nanocatalyst (1)

In our preliminary experiments, the catalytic activity of as prepared catalyst **1** was evaluated in the formation of

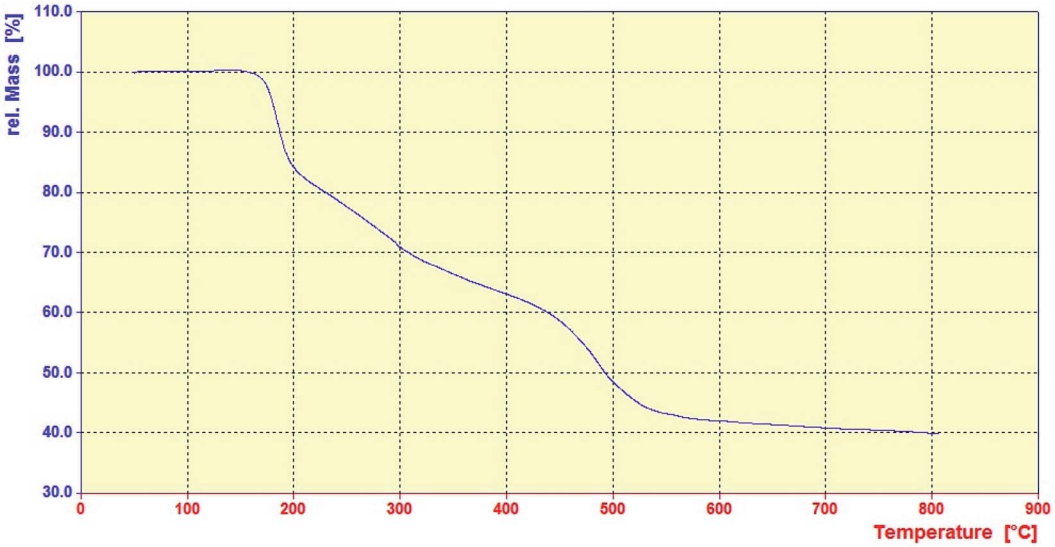

Fig. 7 TGA curve of the magnetic Fe_3O_4@SiO_2–APTS–EDTA–asparagine nanomaterial (**1**).

dihydropyrimidin-2(1*H*)-one derivatives by the Biginelli condensation. For this purpose, reaction conditions were optimized using the equimolar mixtures of urea (**2**, 1 mmol), 4-chlorobenzaldehyde (**3a**, 1 mmol) and ethyl acetoacetate (**4a**, 1 mmol) as the model reaction. In a systematic screening, the reaction conditions were investigated precisely by considering of several crucial variables such as catalyst loading, reaction time, solvent and reaction temperature, as given in Table 1. Initially, in the absence of any catalyst and solvent, the progress of model reaction was slow and the yield of the 9-(4-chlorophenyl)-3,3,6,6-tetramethyl-3,4,6,7,9,10-hexahydroacridine-1,8(2*H*,5*H*)-dione (**5a**) was trace, even after a long time (Table 1,

Table 1 Optimization of conditions in the model reaction of urea (**2**), 4-chlorobenzaldehyde (**3a**), ethyl acetoacetate (**4a**), under different conditions in the presence of Fe_3O_4@SiO_2–APTS–EDTA–asparagine nanocatalyst (**1**)[a]

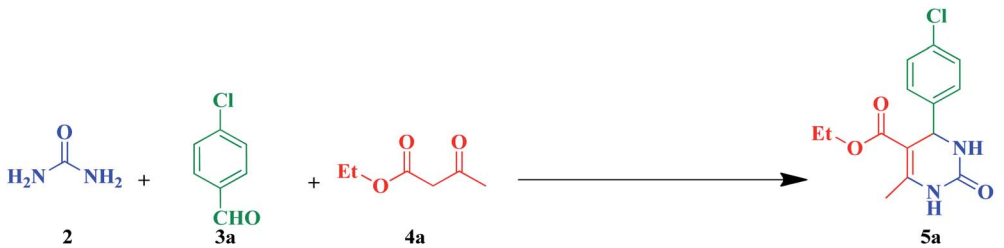

2 **3a** **4a** **5a**

Entry	Catalyst	Solvent	Temperature (°C)	Time (min)	Yield[b] (%) **5a**
1	—	Solvent-free	r.t	30	Trace
2	Fe_3O_4@SiO_2–APTS–EDTA–asparagine	Solvent-free	r.t	30	85
3	Fe_3O_4@SiO_2–APTS–EDTA–asparagine	Solvent-free	40	25	91
4	**Fe_3O_4@SiO_2–APTS–EDTA–asparagine**	**Solvent-free**	**60**	**20**	**95**
5	Fe_3O_4@SiO_2–APTS–EDTA–asparagine	EtOH	r.t	20	65
6	Fe_3O_4@SiO_2–APTS–EDTA–asparagine	EtOH	Reflux	20	85
7	Fe_3O_4@SiO_2–APTS–EDTA–asparagine	MeOH	r.t	40	45
8	Fe_3O_4@SiO_2–APTS–EDTA–asparagine	MeOH	Reflux	40	55
9	Fe_3O_4@SiO_2–APTS–EDTA–asparagine	H_2O	r.t	30	60
10	Fe_3O_4@SiO_2–APTS–EDTA–asparagine	H_2O	Reflux	30	65
11	Fe_3O_4@SiO_2–APTS–EDTA–asparagine	EtOH/H_2O (1 : 1)	r.t	20	63
12	Fe_3O_4@SiO_2–APTS–EDTA–asparagine	EtOH/H_2O (1 : 1)	Reflux	20	70
13	Fe_3O_4@SiO_2–APTS–EDTA–asparagine	DMF	r.t	30	55
14	Fe_3O_4@SiO_2–APTS–EDTA–asparagine	DMF	Reflux	30	65
15	EDTA	Solvent-free	60	20	75
16	Asparagine	Solvent-free	60	20	65

[a] Reaction conditions: urea (**2**, 1 mmol), 4-chlorobenzaldehyde (**3a**, 1 mmol), ethyl acetoacetate (**4a**, 1 mmol), Fe_3O_4@SiO_2–APTS–EDTA–asparagine (**1**) and solvent (3 mL, if not otherwise stated). [b] Isolated yield.

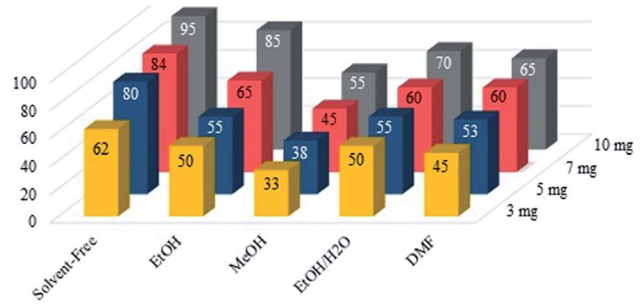

Fig. 8 Effect of solvent and the amount of Fe_3O_4@SiO_2–APTS–EDTA–asparagine nanocatalyst (**1**) on the model reaction.

entry 1). Then, in the presence of very low amount of Fe_3O_4@SiO_2–APTS–EDTA–asparagine (**1**) loading, as a nanocatalyst, a good yield of the desired product **5a** was obtained under solvent-free conditions at room temperature (Table 1, entry 2). To investigate the effect of reaction temperature on the yield of desired product, it was increased to 40 and 60 °C in next experiments (Table 1, entries 3 and 4). Afterward, the model reaction was performed with lower catalyst **1** loading under solvent-free conditions as well as polar and non-polar solvents. Furthermore, the effect of temperature and different solvents was investigated (Table 1, entries 5–14). Also, the model reactions in the presence of EDTA and asparagine were separately investigated, but lower yields of the desired product **5a** were isolated (Table 1, entries 15 and 16).

Following the steps of optimizing the reaction conditions, the effect of different solvents and amount of catalyst loadings are summarized in Fig. 8. The model reaction was investigated under solvent-free conditions and different solvents such as EtOH, MeOH, EtOH/H_2O (1 : 1), and DMF using Fe_3O_4@SiO_2–APTS–EDTA–asparagine nanocatalyst (**1**) with different loading of the catalyst **1**. According to the obtained findings summarized in Table 1 and Fig. 8, the optimum reaction conditions were found to be 10 mg of Fe_3O_4@SiO_2–APTS–EDTA–asparagine nanocatalyst (**1**) loading under solvent-free conditions at 60 °C.

After the above experiments, the scope of reaction was expanded by using aromatic aldehydes having electron-withdrawing or electron-donating groups under the optimized conditions. The results are summarized in Table 2. As observed, for this novel magnetic heterogeneous catalytic system the reaction rate of aldehydes with electron-donating groups was generally slower than electron-withdrawing ones and required more time to complete their reaction. An alternative variation in this reaction was accomplished by utilizing methyl acetoacetate (**4b**) instead of ethyl acetoacetate (**4a**) for the synthesis of different Biginelli products. It is worth noting that all the reactions afforded very good to excellent yields under solvent-free conditions in short reaction times.

The proposed mechanism for the synthesis of 3,4-dihydropyrimidin-2(1*H*)-one derivatives in the presence of Fe_3O_4@SiO_2–APTS–EDTA–asparagine nanocatalyst (1)

The proposed mechanism based on the three-component strategy for synthesis of 3,4-dihydropyrimidin-2(1*H*)-one derivatives catalyzed by the Fe_3O_4@SiO_2–APTS–EDTA–asparagine nanocatalyst (**1**) is presented in Scheme 2. At first, the carbonyl group of aldehyde is activated by the Fe_3O_4@SiO_2–APTS–EDTA–asparagine (**1**) to form the intermediate (**II**) through condensation through the condensation with urea (**2**). Afterward, the iminium intermediate (**IV**) is produced after losing of the H_2O molecule in the presence of the magnetic nanocatalyst. Next, intermediate (**IV**) reacts with the enol form of alkyl acetoacetate (**4**) and the corresponding intermediate (**V**) is generated. Then, intramolecular cyclization occurs which is followed by dehydration of the intermediate (**VI**). At the end of the catalytic cycle, 3,4-dihydropyrimidin-2(1*H*)-ones are produced and the catalyst (**1**) is recycled.

Green chemistry metrics

In this part of our research, green chemistry metrics for the synthesis of 3,4-dihydropyrimidin-2(1*H*)-one by the Fe_3O_4@SiO_2–APTS–EDTA–asparagine nanocatalyst (**1**) were calculated and the results are summarized in Table 3.[114,115] Hence, several parameters of the green chemistry approach such as environmental factor (*E* factor), process mass intensity, reaction mass efficiency, carbon efficiency, and atom economy were evaluated and compared to the ideal values.[116] As presented in Table 3, all calculated values are close to the ideal values and were reported in ESI.†

Reusability of the Fe_3O_4@SiO_2–APTS–EDTA–asparagine nanocatalyst (1)

One of the critical scales in catalytic processes is recyclability and reusability of the catalyst. For evaluation of this parameter, the model reaction was examined using the fresh Fe_3O_4@SiO_2–APTS–EDTA–asparagine (**1**) for five runs. At the end of each run, the catalyst **1** was removed using an external magnet and the recycled catalyst was washed with dry toluene, dried and used in a subsequent model reaction. The obtained results are summarized in Fig. 9. Considering the results of isolated yields of products, the catalytic activity of Fe_3O_4@SiO_2–APTS–EDTA–asparagine nanocatalyst (**1**) after five runs is slightly reduced, which demonstrates proper conservancy of the catalytic activity after recycling.

Comparative study of the Fe_3O_4@SiO_2–APTS–EDTA–asparagine nanocatalyst (1) and other catalysts for the Biginelli reaction

In order to compare the optimal catalytic activity and reaction conditions of the Fe_3O_4@SiO_2–APTS–EDTA–asparagine nanocatalyst (**1**) with previously reported catalysts for the three-component Biginelli reaction, we compared reaction conditions and yield of the desired product (**5a**) in Table 4. As it can be observed from data in Table 4, all catalytic systems are capable of producing the desired product in satisfactory yields but Fe_3O_4@SiO_2–APTS–EDTA–asparagine nanocatalyst (**1**) in terms of yield and time factors, the reaction temperature, solvent and amount of catalyst loading demonstrates better performance than the other catalysts. Furthermore, additional advantage of this protocol is its easy separation from the crude

Table 2 Scope of the synthesis of different 3,4-dihydropyrimidin-2(1*H*)-one derivatives **5a–t** catalyzed by Fe_3O_4@SiO_2–APTS–EDTA–asparagine nanomaterial (**1**) under the optimized conditions[a]

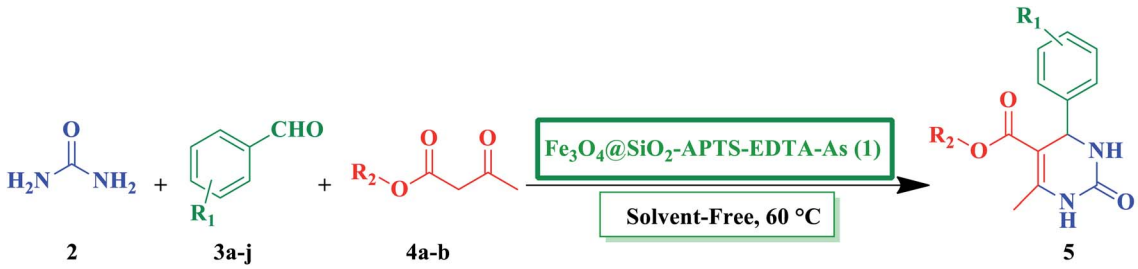

(Eq. 2)

Entry	ArCHO	R_2	Product	Time (min)	Yield[b] (%)	M.p. (°C)	M.p. (°C) (Lit.)
1	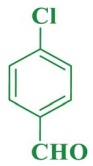 **3a**	Et	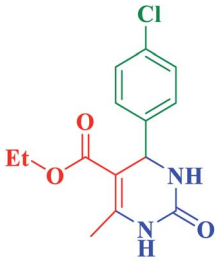 **5a**	20	95	210–212	210–212 (ref. 86)
2	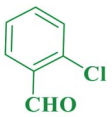 **3b**	Et	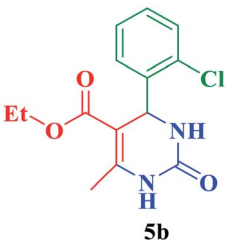 **5b**	25	90	212–214	213–215 (ref. 109)
3	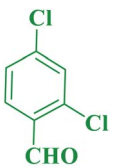 **3c**	Et	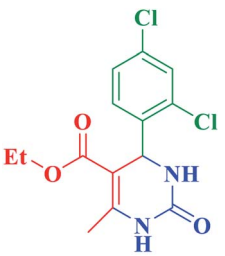 **5c**	25	92	250–252	252–255 (ref. 110)
4	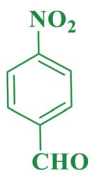 **3d**	Et	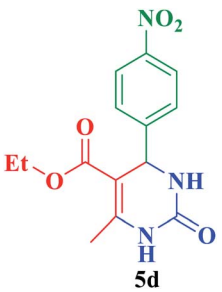 **5d**	45	85	208–210	208–210 (ref. 111)

Table 2 (*Contd.*)

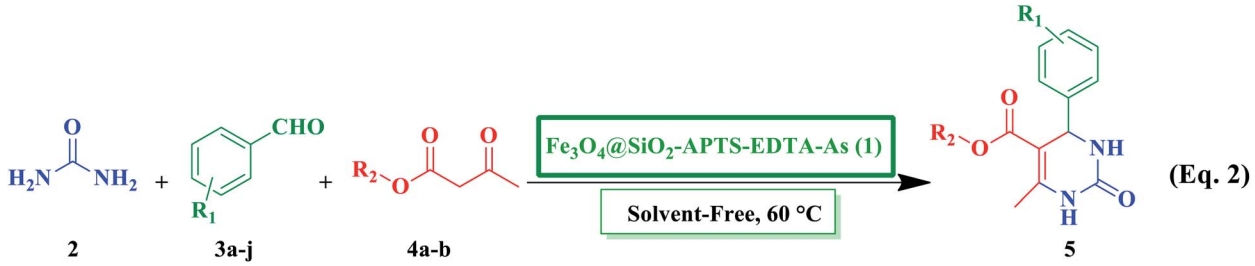

Entry	ArCHO	R_2	Product	Time (min)	Yield[b] (%)	M.p. (°C)	M.p. (°C) (Lit.)
5	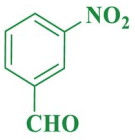 3e	Et	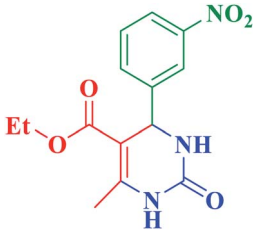 5e	45	87	211–212	212 (ref. 110)
6	 3f	Et	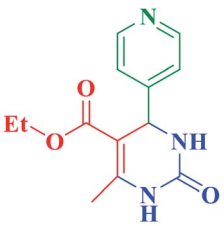 5f	40	85	209–210	210 (ref. 112)
7	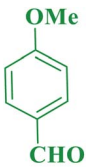 3g	Et	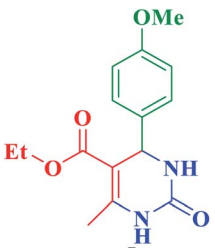 5g	35	89	208–209	206–208 (ref. 85)
8	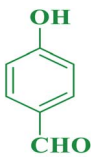 3h	Et	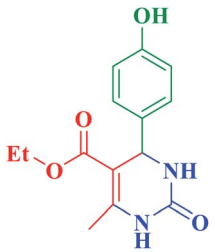 5h	35	87	224–226	225–226 (ref. 72)
9	 3i	Et	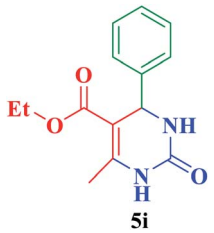 5i	35	88	202–204	201–203 (ref. 109)

Table 2 (*Contd.*)

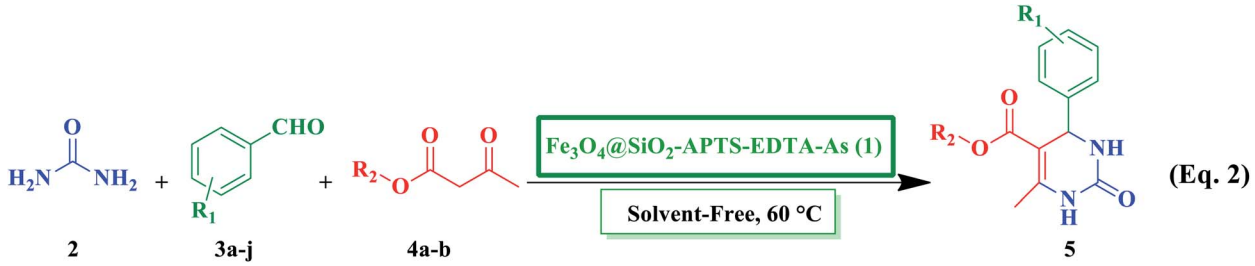

Entry	ArCHO	R_2	Product	Time (min)	Yield[b] (%)	M.p. (°C)	M.p. (°C) (Lit.)
10	 3j	Et	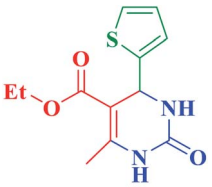 5j	45	88	218–220	220–221 (ref. 113)
11	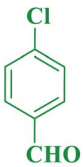 3a	Me	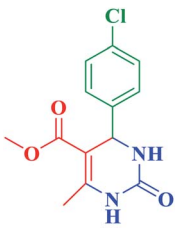 5k	20	94	206–205	203–206 (ref. 114)
12	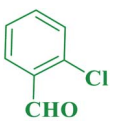 3b	Me	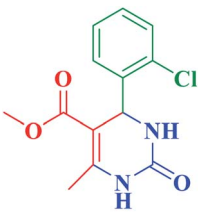 5l	25	89	226–224	226–229 (ref. 114)
13	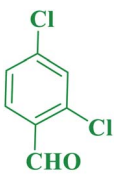 3c	Me	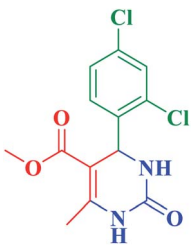 5m	25	92	252–254	254–255 (ref. 111)
14	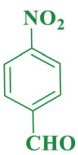 3d	Me	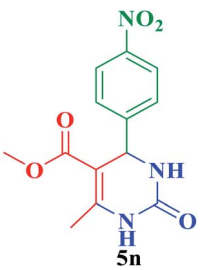 5n	45	85	238–236	239–240 (ref. 115)

Table 2 (*Contd.*)

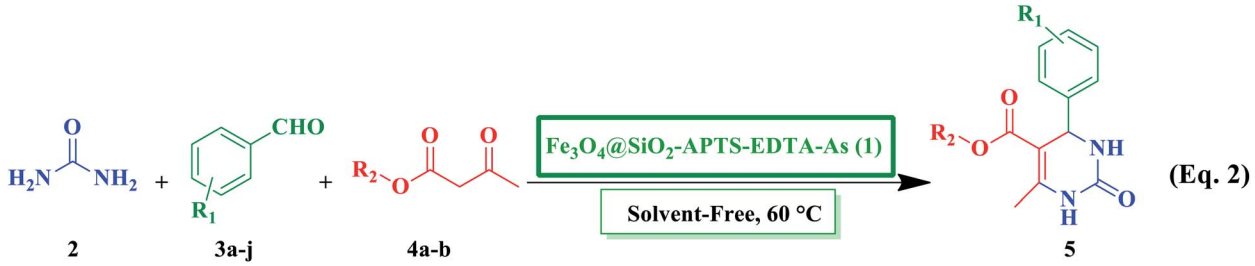

Entry	ArCHO	R_2	Product	Time (min)	Yield[b] (%)	M.p. (°C)	M.p. (°C) (Lit.)
15	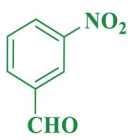 3e	Me	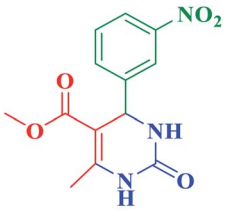 5o	45	86	274–272	276–279 (ref. 114)
16	 3f	Me	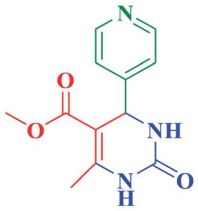 5p	45	85	219–218	220 (ref. 112)
17	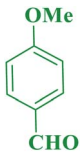 3g	Me	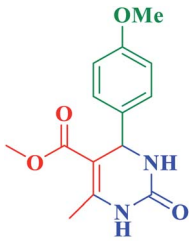 5q	35	88	204–202	198–199 (ref. 115)
18	 3h	Me	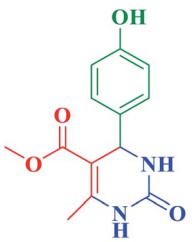 5r	35	87	230–228	230–231 (ref. 115)
19	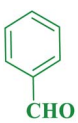 3i	Me	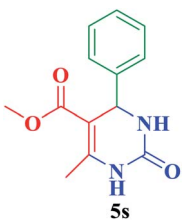 5s	35	87	211–212	210–212 (ref. 109)

Table 2 (*Contd.*)

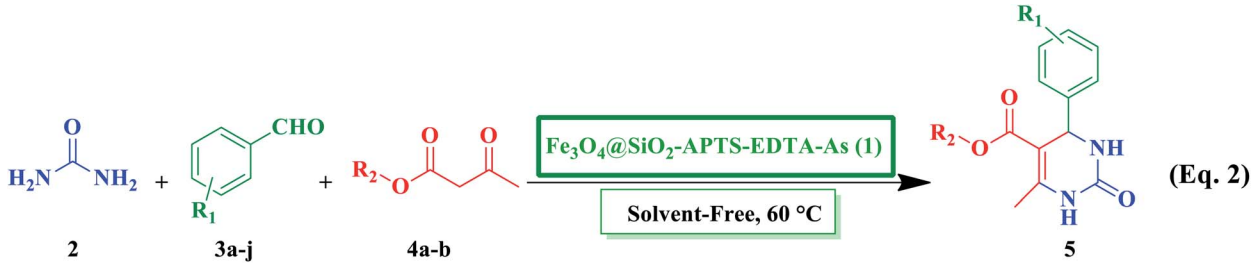

Entry	ArCHO	R_2	Product	Time (min)	Yield[b] (%)	M.p. (°C)	M.p. (°C) (Lit.)
20	 3j	Me	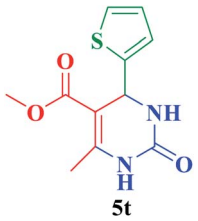 5t	45	88	226–224	226–227 (ref. 113)

[a] Reaction conditions: urea (**2**, 1 mmol), aldehydes (**3a–j**, 1 mmol), ethyl acetoacetate or methyl acetoacetate (**4a–b**, 1 mmol) and catalyst (**1**, 10 mg) under solvent-free conditions at 60 °C. [b] Isolated yield.

reaction mixture by using an external magnet compared to the most of reported heterogeneous catalytic systems.

Experimental

Chemicals and instrumentation

Ferric chloride ($FeCl_3 \cdot 6H_2O$), ferrous chloride tetrahydrate ($FeCl_2 \cdot 4H_2O$), (3-aminopropyl)triethoxysilane (APTS, 99%), tetraethyl orthosilicate (TEOS, 99%), ammonia (25 wt%), EDTA (MW = 292.24 g mol^{-1}) and L-asparagine (MW = 132.12 g mol^{-1}) were purchased from Merck and used without further purification. Urea, ethyl- or methyl acetoacetate and aromatic aldehydes were purchased from international chemical companies including Merck and Sigma-Aldrich. The analytical TLC experiments were accomplished using Merck Kieselgel 60 F-254 Al-plates and then visualized by UV light and iodine vapour. Melting points of the products were measured on an Electrothermal 9100 apparatus and uncorrected. The functional groups of the samples were identified by FT-IR spectroscopy on a PerkinElmer, Frontier FT-MIR spectrometer in the range of 600–4000 cm^{-1} using KBr discs. The morphology of the nano-catalyst was observed by FESEM TESCAN-MIRA3 and TEM Philips EM 208S. TGA curves of the Fe_3O_4@SiO_2–APTS–EDTA–asparagine (**1**) were recorded by using a Bahr company STA 504 instrument. X-ray diffraction (XRD) pattern of the catalyst **1** was taken by using the Bruker D8 Advance device. The composition of the catalyst was determined by energy-dispersive X-ray (EDX) spectroscopy using a Numerix DXP-X10P instrument. Magnetization measurements were carried out on a BHV-55 vibrating sample magnetometer (VSM). ^{1}H NMR spectra of the isolated products were recorded at 500 MHz using a Varian-INOVA spectrometer.

General procedure for preparation of the magnetic Fe_3O_4 nanoparticles

Preparation of the Fe_3O_4 nanoparticles were accomplished according to a reported general method.[118] In this procedure, in a 100 mL round-bottomed flask $FeCl_3 \cdot 6H_2O$ (4.6 g, 0.017 mol) and $FeCl_2 \cdot 4H_2O$ (2.3 g, 0.011 mol) were dissolved in deionized water (60 mL) and stirred for 30 min. Subsequently, aqueous NH_3 (10 mL) was added dropwise into the mixture and heated to 40 °C under N_2 atmosphere for 2 h. The black mixture was decanted and Fe_3O_4 MNPs precipitates were separated from the remaining mixture using an external magnet, washed five times with deionized water and EtOH, and dried in the oven at 50 °C for 24 h.

General procedure for preparation of the silica-coated magnetic nanoparticles (Fe_3O_4@SiO_2)

In accordance to the modified Stöber method, silica-coated Fe_3O_4 nanoparticles (Fe_3O_4@SiO_2) were prepared by a solvothermal procedure.[119] For this purpose, the Fe_3O_4 MNPs (1.0 g) were dispersed in 30 mL of distilled water and ultrasonicated for 30 min. Then, a mixture of aqueous NH_3 (2 mL) and EtOH (40 mL) were added dropwise to the obtained mixture and ultrasonicated for 30 min. Afterward, a mixture of TEOS (2 mL) and EtOH (40 mL) were added slowly to the suspension solution under continuous stirring for 24 h at 60 °C. Eventually, the Fe_3O_4@SiO_2 core–shell MNPs were collected using an external magnet, washed with deionized water and EtOH and dried in an oven at 50 °C for 5 h.

Modification of the Fe_3O_4@SiO_2 NPs by (3-aminopropyl) triethoxysilane (Fe_3O_4@SiO_2–APTS)

The Fe_3O_4@SiO_2 core–shell MNPs were modified with (3-aminopropyl)triethoxysilane (APTS) using a typical modified

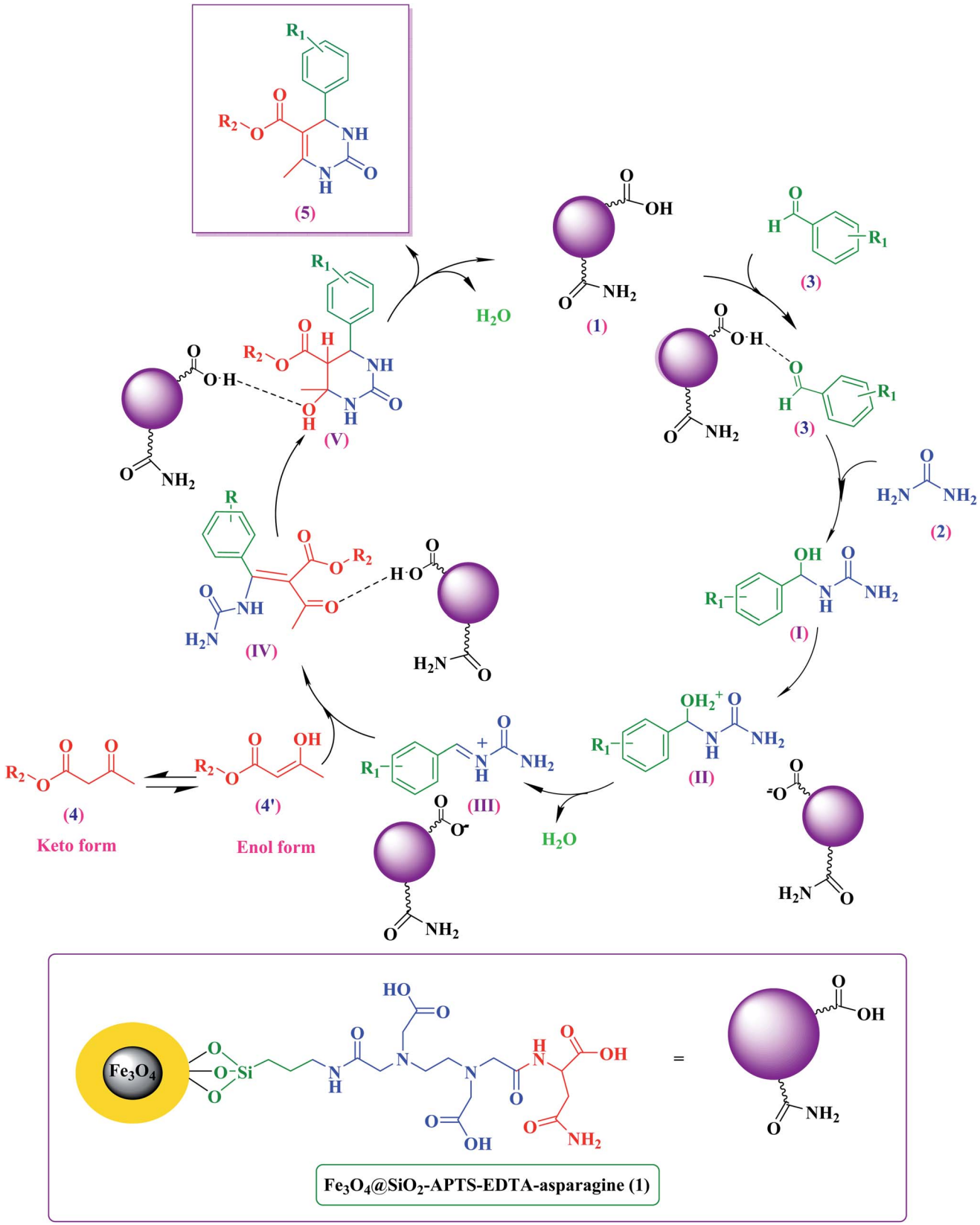

Scheme 2 The proposed mechanism for the synthesis of 3,4-dihydropyrimidin-2(1*H*)-one derivatives using ethyl acetoacetate or methyl acetoacetate in the presence of Fe_3O_4@SiO_2–APTS–EDTA–asparagine nanocatalyst (**1**).

Table 3 Measurement of green chemistry metrics for compound 5a

Entry	Parameters of the green approach	Ideal value	Calculated values
1	*E* factor	0	0.16
2	Atom economy (AE %)	100%	89.1%
3	Carbon efficiency (CE %)	100%	96%
4	Process mass intensity (PMI)	1	1.16
5	Reaction mass efficiency (RME %)	100%	85.5%

method.[120] Briefly, the Fe_3O_4@SiO_2 NPs (1.0 g) were ultrasonicated in 30 mL dried toluene. Subsequently, (3-aminopropyl)triethoxysilane (APTS, 2.0 mL) was added to the obtained mixture and stirred at 105 °C for 24 h. The resulting mixture was allowed to cool down to room temperature and then obtained precipitate was filtered off. After washing with dry toluene, the obtained MNPs were separated and dried at 60 °C for 12 h in a vacuum oven to prepare the Fe_3O_4@SiO_2–APTS MNPs.

Preparation of the EDTA functionalized magnetic nanoparticles (Fe_3O_4@SiO_2–APTS–EDTA)

In a round-bottom flask, the magnetic Fe_3O_4@SiO_2–APTS NPs (1.0 g) were added to dry toluene (25 mL) and dispersed using ultrasonic for 15 min. Then, EDTA dianhydride (1.0 g) – synthesized according to the procedure described by Repo *et al.*[121] – and acetic anhydride were added to the mixture and stirred at 80 °C under N_2 atmosphere for 24 h. The obtained magnetic Fe_3O_4@SiO_2–APTS–EDTA NPs were washed five times with EtOH followed by drying at 60 °C for 6 h in a vacuum oven.

Preparation of the L-asparagine grafted on the EDTA-modified Fe_3O_4@SiO_2 core–shell magnetic nanoparticles (Fe_3O_4@SiO_2–APTS–EDTA–asparagine, 1)

In the last step, the magnetic Fe_3O_4@SiO_2–APTS–EDTA NPs were dispersed in 25 mL of dry toluene and L-asparagine (1.0 g) was added to the magnetic mixture and stirred under N_2 atmosphere and reflux conditions for 24 h. The magnetic precipitates were separated using an external magnet and washed with EtOH three times. After drying of the obtained precipitates in an oven at 60 °C for 3 h, the brown powder of Fe_3O_4@SiO_2–APTS–EDTA–asparagine nanocatalyst (**1**) was obtained.

General procedure for the synthesis of 3,4-dihydropyrimidin-2(1*H*)-one (5a–t) catalyzed by Fe_3O_4@SiO_2–APTS–EDTA–asparagine nanomaterial (1)

A mixture of urea (**2**, 1.0 mmol), aromatic aldehyde (**3**, 1.0 mmol), ethyl or methyl acetoacetate (**4a–b**, 1.0 mmol) and Fe_3O_4@SiO_2–APTS–EDTA–asparagine (**1**, 10 mg) were heated under solvent-free conditions at 60 °C for an appropriate time indicated in Table 2. After completion of the reaction, as monitored by TLC [eluent: *n*-hexane : EtOAc; 3 : 1], the catalyst was separated using an external magnet and the residue was

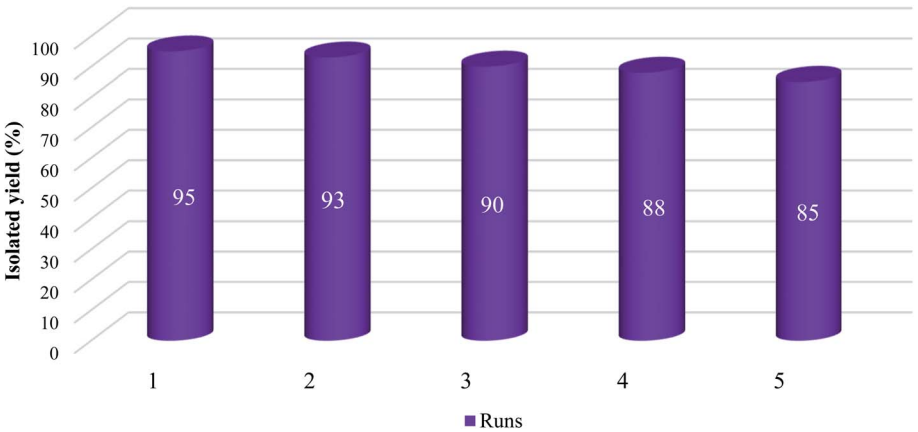

Fig. 9 Reusability of the Fe_3O_4@SiO_2–APTS–EDTA–asparagine nanocatalyst (**1**) for the synthesis of **5a**.

Table 4 Comparative results of catalysts for the synthesis of 5a

Entry	Catalyst	Catalyst loading (mg)	Reaction conditions	Time (min)	Yield (%)
1	Zn MOF	10	Solvent-free/60 °C	120	91 (ref. 78)
2	PANI-$FeCl_3$	200	CH_3CN/reflux	1440	83 (ref. 117)
3	MCM-41-APS-PMDANHSO$_3$H	15	Solvent-free/80 °C	35	96 (ref. 87)
4	Fe_3O_4@SiO_2–APTMS–$Fe(OH)_2$	10	Neat/80 °C	15	95 (ref. 81)
5	Zirconium(IV)–salophen perfluorooctanesulfonate	5	Solvent-free/90 °C	30	96 (ref. 82)
6	Fe_3O_4@SiO_2–APTS–EDTA–asparagine	10	Solvent-free/60 °C	20	95 (this work)

concentrated to afford the crude product. Finally, the crude product was recrystallized from EtOH to obtain the pure products **5a–t**.

Conclusion

In summary, the novel and thermally stable L-asparagine grafted on the 3-aminopropyl-modified Fe_3O_4@SiO_2 core–shell magnetic nanoparticles using the EDTA linker (Fe_3O_4@SiO_2–APTS–EDTA–asparagine) was prepared for the first time. The nano-ordered Fe_3O_4@SiO_2–APTS–EDTA–asparagine heterogeneous multifunctional organocatalyst was used for highly efficient, facile, and green and sustainable synthesis of a wide range of 3,4-dihydropyrimidin-2(1*H*)-one derivatives in a one-pot and three-component protocol through cyclocondensation of alkyl acetoacetate, urea and various aldehydes under solvent-free conditions at 60 °C. Consistency with the ideal values of green chemistry parameters, easy work up procedure, good to excellent yields in short reaction times, fast separation and recyclability of the catalyst are the additional advantages of this new methodology.

Conflicts of interest

There are no conflicts to declare.

Acknowledgements

We thank The Research Council of Iran University of Science and Technology (IUST), Tehran, Iran (Grant No. 160/20969) for their support. We would also like to acknowledge the support of Iran Nanotechnology Initiative Council (INIC), Iran.

References

1 P. T. Anastas and J. B. Zimmerman, *Green Chem.*, 2019, **21**, 6545–6566.
2 J. H. Clark, in *Green and Sustainable Medicinal Chemistry: Methods, Tools and Strategies for the 21st Century Pharmaceutical Industry*, The Royal Society of Chemistry, 2016, pp. 1–11, DOI: 10.1039/9781782625940-00001.
3 R. A. Sheldon, *ACS Sustainable Chem. Eng.*, 2018, **6**, 32–48.
4 C.-J. Li and P. T. Anastas, *Chem. Soc. Rev.*, 2012, **41**, 1413–1414.
5 H. C. Erythropel, J. B. Zimmerman, T. M. de Winter, L. Petitjean, F. Melnikov, C. H. Lam, A. W. Lounsbury, K. E. Mellor, N. Z. Janković and Q. Tu, *Green Chem.*, 2018, **20**, 1929–1961.
6 K. N. Ganesh, D. Zhang, S. J. Miller, K. Rossen, P. J. Chirik, M. C. Kozlowski, J. B. Zimmerman, B. W. Brooks, P. E. Savage, D. T. Allen and A. M. Voutchkova-Kostal, *Org. Process Res. Dev.*, 2021, **25**, 1455–1459.
7 Z. Jin, C. Yan, H. Chu, Q. Huang and Z. Wang, *RSC Adv.*, 2022, **12**, 10460–10466.
8 R. A. Hernandez R, K. Burchell-Reyes, A. P. C. A. Braga, J. K. Lopez and P. Forgione, *RSC Adv.*, 2022, **12**, 6396–6402.
9 V. V. Phatake and B. M. Bhanage, *Tetrahedron Lett.*, 2021, **68**, 152940.
10 M. Bilal, Y. Zhao, T. Rasheed and H. M. Iqbal, *Int. J. Biol. Macromol.*, 2018, **120**, 2530–2544.
11 M. A. Zolfigol, R. Ayazi-Nasrabadi, S. Baghery, V. Khakyzadeh and S. Azizian, *J. Mol. Catal. A: Chem.*, 2016, **418–419**, 54–67.
12 V. Gdovinová, N. Tomašovičová, S.-C. Jeng, K. Zakutanská, P. Kula and P. Kopčanský, *J. Mol. Liq.*, 2019, **282**, 286–291.
13 L. L. Félix, B. Sanz, V. Sebastián, T. Torres, M. H. Sousa, J. Coaquira, M. Ibarra and G. F. Goya, *Sci. Rep.*, 2019, **9**, 1–11.
14 A. Moghanizadeh, F. Ashrafizadeh, J. Varshosaz and A. Ferreira, *Sci. Rep.*, 2021, **11**, 1–13.
15 C. Bai, P. Hu, N. Liu, G. Feng, D. Liu, Y. Chen, M. Ma, N. Gu and Y. Zhang, *ACS Appl. Nano Mater.*, 2020, **3**, 3585–3595.
16 C. Lu, L. Han, J. Wang, J. Wan, G. Song and J. Rao, *Chem. Soc. Rev.*, 2021, **50**, 11870–11965.
17 K. Yan, P. Li, H. Zhu, Y. Zhou, J. Ding, J. Shen, Z. Li, Z. Xu and P. K. Chu, *RSC Adv.*, 2013, **3**, 10598–10618.
18 A. S. Garanina, V. A. Naumenko, A. A. Nikitin, E. Myrovali, A. Y. Petukhova, S. V. Klimyuk, Y. A. Nalench, A. R. Ilyasov, S. S. Vodopyanov and A. S. Erofeev, *Nanomed. Nanotechnol. Biol. Med.*, 2020, **25**, 102171.
19 G. C. Lavorato, R. Das, J. A. Masa, M.-H. Phan and H. Srikanth, *Nanoscale Adv.*, 2021, **3**, 867–888.
20 Z. Wang, J. Guo, J. Ma and L. Shao, *J. Mater. Chem. A*, 2015, **3**, 19960–19968.
21 R. Mrówczyński, A. Nan and J. Liebscher, *RSC Adv.*, 2014, **4**, 5927–5952.
22 S. Saranya, T. Aneeja, M. Neetha and G. Anilkumar, *Appl. Organomet. Chem.*, 2020, **34**, e5991.
23 Q. Zhang, X. Yang and J. Guan, *ACS Appl. Nano Mater.*, 2019, **2**, 4681–4697.
24 M. Ishani, M. G. Dekamin and Z. Alirezvani, *J. Colloid Interface Sci.*, 2018, **521**, 232–241.
25 S. Karami, M. G. Dekamin, E. Valiey and P. Shakib, *New J. Chem.*, 2020, **44**, 13952–13961.
26 Z. Alirezvani, M. G. Dekamin and E. Valiey, *Sci. Rep.*, 2019, **9**, 17758.
27 G. Simonsen, M. Strand and G. Øye, *J. Petrol. Sci. Eng.*, 2018, **165**, 488–495.
28 K. Zhou, X. Zhou, J. Liu and Z. Huang, *J. Petrol. Sci. Eng.*, 2020, **188**, 106943.
29 S. P. Yeap, J. Lim, B. S. Ooi and A. L. Ahmad, *J. Nanoparticle Res.*, 2017, **19**, 1–15.
30 J. Chen, Y. Ren, H. Li, W. Yang, Q. Wu, Y. Zhao, Q. Jiao, Y. Lu and D. Shi, *ACS Omega*, 2020, **5**, 23062–23069.
31 H. FaniMoghadam, M. G. Dekamin and N. Rostami, *Res. Chem. Intermed.*, 2022, **48**, 3061–3089.
32 A. Trifonov, A. Stemmer and R. Tel-Vered, *Bioelectrochemistry*, 2021, **137**, 107640.
33 L. M. Martínez-Prieto, J. Marbaix, J. M. Asensio, C. Cerezo-Navarrete, P.-F. Fazzini, K. Soulantica, B. Chaudret and A. Corma, *ACS Appl. Nano Mater.*, 2020, **3**, 7076–7087.
34 M. Ziegler-Borowska, *Int. J. Biol. Macromol.*, 2019, **136**, 106–114.

35 A. Khazaei, M. Khazaei and M. Nasrollahzadeh, *Tetrahedron*, 2017, **73**, 5624–5633.
36 E. S. D. T. de Mendonça, A. C. B. de Faria, S. C. L. Dias, F. F. Aragón, J. C. Mantilla, J. A. Coaquira and J. A. Dias, *Surface. Interfac.*, 2019, **14**, 34–43.
37 Y. H. Gad and A. M. Elbarbary, *Appl. Organomet. Chem.*, 2021, **35**, e6258.
38 U. K. Sharma, P. Ranjan, E. V. Van der Eycken and S.-L. You, *Chem. Soc. Rev.*, 2020, **49**, 8721–8748.
39 M. G. Dekamin, M. Eslami and A. Maleki, *Tetrahedron*, 2013, **69**, 1074–1085.
40 M. Keshavarz, M. G. Dekamin, M. Mamaghani and M. Nikpassand, *Sci. Rep.*, 2021, **11**, 14457.
41 N. Rostami, M. G. Dekamin, E. Valiey and H. Fanimoghadam, *Sci. Rep.*, 2022, **12**, 8642.
42 P. Slobbe, E. Ruijter and R. V. Orru, *MedChemComm*, 2012, **3**, 1189–1218.
43 M. R. Khumalo, S. N. Maddila, S. Maddila and S. B. Jonnalagadda, *RSC Adv.*, 2019, **9**, 30768–30772.
44 H. Ebrahimiasl, D. Azarifar, J. Rakhtshah, H. Keypour and M. Mahmoudabadi, *Appl. Organomet. Chem.*, 2020, **34**, e5769.
45 M. G. Dekamin, M. Azimoshan and L. Ramezani, *Green Chem.*, 2013, **15**, 811–820.
46 Z. Alirezvani, M. G. Dekamin and E. Valiey, *ACS Omega*, 2019, **4**, 20618–20633.
47 E. Valiey, M. G. Dekamin and Z. Alirezvani, *Int. J. Biol. Macromol.*, 2019, **129**, 407–421.
48 A. Akbari, M. G. Dekamin, A. Yaghoubi and M. R. Naimi-Jamal, *Sci. Rep.*, 2020, **10**, 10646.
49 S. E. John, S. Gulati and N. Shankaraiah, *Org. Chem. Front.*, 2021, **8**, 4237–4287.
50 R. C. Cioc, E. Ruijter and R. V. Orru, *Green Chem.*, 2014, **16**, 2958–2975.
51 S. Basu, S. Chatterjee, A. Bhaumik and C. Mukhopadhyay, *Appl. Organomet. Chem.*, 2021, **35**, e6426.
52 Â. d. Fátima, T. C. Braga, B. S. Terra and L. d. S. Neto, in *Green Synthetic Approaches for Biologically Relevant Heterocycles*, ed. G. Brahmachari, Elsevier, 2nd edn, 2021, pp. 253–300.
53 D. S. Aher, K. R. Khillare, L. D. Chavan and S. G. Shankarwar, *RSC Adv.*, 2021, **11**, 2783–2792.
54 N. Kaur, in *Metal and Nonmetal Assisted Synthesis of Six-Membered Heterocycles*, ed. N. Kaur, Elsevier, 2020, pp. 183–241.
55 H. Nagarajaiah, A. Mukhopadhyay and J. N. Moorthy, *Tetrahedron Lett.*, 2016, **57**, 5135–5149.
56 I. Essid, K. Lahbib, W. Kaminsky, C. B. Nasr and S. Touil, *J. Mol. Struct.*, 2017, **1142**, 130–138.
57 F.-J. Meng, L. Shi, G.-S. Feng, L. Sun and Y.-G. Zhou, *J. Org. Chem.*, 2019, **84**, 4435–4442.
58 M. Matias, G. Campos, A. O. Santos, A. Falcão, S. Silvestre and G. Alves, *RSC Adv.*, 2016, **6**, 84943–84958.
59 K. Venkatapathy, C. Magesh, G. Lavanya, P. Perumal and R. Sathishkumar, *New J. Chem.*, 2019, **43**, 10989–11002.
60 A. Shaabani, A. Bazgir and F. Teimouri, *Tetrahedron Lett.*, 2003, **44**, 857–859.
61 A. E. Huseynzada, C. Jelsch, H. N. Akhundzada, S. Soudani, C. B. Nasr, F. Doria, U. A. Hasanova, M. Freccero, Z. Gakhramanova, K. Ganbarov and B. Najafov, *J. Mol. Struct.*, 2021, **1241**, 130678.
62 J. Chen, D. Wu, F. He, M. Liu, H. Wu, J. Ding and W. Su, *Tetrahedron Lett.*, 2008, **49**, 3814–3818.
63 S. Khademinia, M. Behzad, A. Alemi, M. Dolatyari and S. M. Sajjadi, *RSC Adv.*, 2015, **5**, 71109–71114.
64 J. Mabry and B. Ganem, *Tetrahedron Lett.*, 2006, **47**, 55–56.
65 M. A. Zolfigol, H. Ghaderi, S. Baghery and L. Mohammadi, *J. Iran. Chem. Soc.*, 2017, **14**, 121–134.
66 A. K. Bose, S. Pednekar, S. N. Ganguly, G. Chakraborty and M. S. Manhas, *Tetrahedron Lett.*, 2004, **45**, 8351–8353.
67 S. Faizan, B. R. Prashantha Kumar, N. Lalitha Naishima, T. Ashok, A. Justin, M. Vijay Kumar, R. Bistuvalli Chandrashekarappa, N. Manjunathaiah Raghavendra, P. Kabadi and L. Adhikary, *Bioorg. Chem.*, 2021, **117**, 105462.
68 R. V. Patil, J. U. Chavan, D. S. Dalal, V. S. Shinde and A. G. Beldar, *ACS Comb. Sci.*, 2019, **21**, 105–148.
69 L. G. do Nascimento, I. M. Dias, G. B. M. de Souza, L. C. Mourão, M. B. Pereira, J. C. V. Viana, L. M. Lião, G. R. de Oliveira and C. G. Alonso, *New J. Chem.*, 2022, **46**, 6091–6102.
70 A. Debache, B. Boumoud, M. Amimour, A. Belfaitah, S. Rhouati and B. Carboni, *Tetrahedron Lett.*, 2006, **47**, 5697–5699.
71 P. Madivalappa Davanagere and B. Maiti, *ACS Omega*, 2021, **6**, 26035–26047.
72 B.-J. Yao, W.-X. Wu, L.-G. Ding and Y.-B. Dong, *J. Org. Chem.*, 2021, **86**, 3024–3032.
73 E. F. Freitas, R. Y. Souza, S. T. A. Passos, J. A. Dias, S. C. L. Dias and B. A. D. Neto, *RSC Adv.*, 2019, **9**, 27125–27135.
74 A. Shaabani, A. Sarvary, A. Rahmati and A. H. Rezayan, *Lett. Org. Chem.*, 2007, **4**, 68–71.
75 R. J. Kalbasi, A. R. Massah and B. Daneshvarnejad, *Appl. Clay Sci.*, 2012, **55**, 1–9.
76 J. Safaei-Ghomi, M. Tavazo and G. H. Mahdavinia, *Ultrason. Sonochem.*, 2018, **40**, 230–237.
77 G. C. O. Silva, J. R. Correa, M. O. Rodrigues, H. G. O. Alvim, B. C. Guido, C. C. Gatto, K. A. Wanderley, M. Fioramonte, F. C. Gozzo, R. O. M. A. de Souza and B. A. D. Neto, *RSC Adv.*, 2015, **5**, 48506–48515.
78 A. Verma, D. De, K. Tomar and P. K. Bharadwaj, *Inorg. Chem.*, 2017, **56**, 9765–9771.
79 U. Patel, B. Parmar, P. Patel, A. Dadhania and E. Suresh, *Mater. Chem. Front.*, 2021, **5**, 304–314.
80 A. Phukan, S. J. Borah, P. Bordoloi, K. Sharma, B. J. Borah, P. P. Sarmah and D. K. Dutta, *Adv. Powder Technol.*, 2017, **28**, 1585–1592.
81 M. Sheykhan, A. Yahyazadeh and L. Ramezani, *Mol. Catal.*, 2017, **435**, 166–173.
82 N. Li, Y. Wang, F. Liu, X. Zhao, X. Xu, Q. An and K. Yun, *Appl. Organomet. Chem.*, 2020, **34**, e5454.
83 C. K. Khatri, D. S. Rekunge and G. U. Chaturbhuj, *New J. Chem.*, 2016, **40**, 10412–10417.

84 M. G. Dekamin, F. Mehdipoor and A. Yaghoubi, *New J. Chem.*, 2017, **41**, 6893–6901.
85 Y. T. Wang, G. M. Tang and Y. S. Wu, *Appl. Organomet. Chem.*, 2020, **34**, e5542.
86 Z. Nasresfahani and M. Z. Kassaee, *Appl. Organomet. Chem.*, 2018, **32**, e4106.
87 E. Valiey, M. G. Dekamin and Z. Alirezvani, *Sci. Rep.*, 2021, **11**, 11199.
88 B. List, *Chem. Rev.*, 2007, **107**, 5413–5415.
89 D. W. C. MacMillan, *Nature*, 2008, **455**, 304–308.
90 P. Kočovský and A. V. Malkov, *Tetrahedron*, 2006, **62**, 255.
91 M. P. van der Helm, B. Klemm and R. Eelkema, *Nat. Rev. Chem.*, 2019, **3**, 491–508.
92 S. Bertelsen and K. A. Jørgensen, *Chem. Soc. Rev.*, 2009, **38**, 2178–2189.
93 T. Yu, Z. Xue, X. Zhao, W. Chen and T. Mu, *New J. Chem.*, 2018, **42**, 16154–16161.
94 K. Zhang, Z. Dai, W. Zhang, Q. Gao, Y. Dai, F. Xia and X. Zhang, *Coord. Chem. Rev.*, 2021, **434**, 213809.
95 N. Danesh, M. Ghorbani and A. Marjani, *Sci. Rep.*, 2021, **11**, 1–23.
96 F. Zhao, E. Repo, D. Yin, L. Chen, S. Kalliola, J. Tang, E. Iakovleva, K. C. Tam and M. Sillanpää, *Sci. Rep.*, 2017, **7**, 1–14.
97 E. Valiey and M. G. Dekamin, *RSC Adv.*, 2022, **12**, 437–450.
98 W. H. Tong, *Cancer Chemother. Pharmacol.*, 2021, 1–2.
99 X. Wang, T. Gao, M. Yang, J. Zhao, F.-L. Jiang and Y. Liu, *New J. Chem.*, 2019, **43**, 3323–3331.
100 G. Saikia, K. Ahmed, C. Rajkhowa, M. Sharma, H. Talukdar and N. S. Islam, *New J. Chem.*, 2019, **43**, 17251–17266.
101 E. Valiey and M. G. Dekamin, *Nanoscale Adv.*, 2022, **4**, 294–308.
102 M. Sam, M. G. Dekamin and Z. Alirezvani, *Sci. Rep.*, 2021, **11**, 2399.
103 S. Ilkhanizadeh, J. Khalafy and M. G. Dekamin, *Int. J. Biol. Macromol.*, 2019, **140**, 605–613.
104 N. Etivand, J. Khalafy and M. G. Dekamin, *Synthesis*, 2020, **52**, 1707–1718.
105 C. Jin, Y. Wang, H. Wei, H. Tang, X. Liu, T. Lu and J. Wang, *J. Mater. Chem. A.*, 2014, **2**, 11202–11208.
106 F. An and B. Gao, *J. Hazard. Mater.*, 2007, **145**, 495–500.
107 S. Kargar, D. Elhamifar and A. Zarnegaryan, *J. Phys. Chem. Solids*, 2020, **146**, 109601.
108 E. Abbaspour-Gilandeh, A. Yahyazadeh and M. Aghaei-Hashjin, *RSC Adv.*, 2018, **8**, 40243–40251.
109 J. Safari and S. Gandomi-Ravandi, *New J. Chem.*, 2014, **38**, 3514–3521.
110 K. M. Bairagi, K. N. Venugopala, P. K. Mondal, R. M. Gleiser, D. Chopra, D. García, B. Odhav and S. K. Nayak, *Chem. Biol. Drug Des.*, 2018, **92**, 1924–1932.
111 M. Majellaro, W. Jespers, A. Crespo, M. J. Núñez, S. Novio, J. Azuaje, R. Prieto-Díaz, C. Gioé, B. Alispahic and J. Brea, *J. Med. Chem.*, 2020, **64**, 458–480.
112 R. Esmaeili, L. Kafi-Ahmadi and S. Khademinia, *J. Mol. Struct.*, 2020, **1216**, 128124.
113 L. G. do Nascimento, I. M. Dias, G. B. Meireles de Souza, I. Dancini-Pontes, N. R. C. Fernandes, P. S. de Souza, G. Roberto de Oliveira and C. G. Alonso, *J. Org. Chem.*, 2020, **85**, 11170–11180.
114 P. J. Dunn, S. Galvin and K. Hettenbach, *Green Chem.*, 2004, **6**, 43–48.
115 P. Singh, P. Yadav, A. Mishra and S. K. Awasthi, *ACS Omega*, 2020, **5**, 4223–4232.
116 D. J. Constable, A. D. Curzons and V. L. Cunningham, *Green Chem.*, 2002, **4**, 521–527.
117 F. Zamani and E. Izadi, *Catal. Commun.*, 2013, **42**, 104–108.
118 B. Wang, Q. Wei and S. Qu, *Int. J. Electrochem. Sci.*, 2013, **8**, 3786–3793.
119 W. Stöber, A. Fink and E. Bohn, *J. Colloid Interface Sci.*, 1968, **26**, 62–69.
120 M. Jafarzadeh, E. Soleimani, P. Norouzi, R. Adnan and H. Sepahvand, *J. Fluorine Chem.*, 2015, **178**, 219–224.
121 E. Repo, T. A. Kurniawan, J. K. Warchol and M. E. Sillanpää, *J. Hazard Mater.*, 2009, **171**, 1071–1080.
122 M. G. Dekamin, Z. Karimi and M. Farahmand, *Catal. Sci. Technol.*, 2012, **2**, 1375–1381.
123 M. G. Dekamin, S. Sagheb-Asl and M. Reza Naimi-Jamal, *Tetrahedron Lett.*, 2009, **50**, 4063–4066.